Cluster-based characterization of multi-dimensional tropospheric ozone variability in coastal regions: an analysis of lidar measurements and model results

Claudia Bernier[1], Yuxuan Wang[1], Guillaume Gronoff[2,3], Timothy Berkoff[2], K. Emma Knowland[4,5], John T. Sullivan[4], Ruben Delgado[6,7], Vanessa Caicedo[6,7], Brian Carroll[2,6]

[1] Department of Earth and Atmospheric Science, University of Houston, Houston, Texas, USA

[2] NASA Langley Research Center, Hampton, VA, 23666, USA

[3] Science Systems and Application Inc., Hampton, VA, 23666, USA

[4] NASA Goddard Space Flight Center, Global Modeling and Assimilation Office, Greenbelt, MD, 20771, USA

[5] Morgan State University, Goddard Earth Science Technology & Research (GESTAR) II, Baltimore, Maryland, USA

[6] Joint Center for Earth Systems Technology, Baltimore, MD, USA

[7] University of Maryland Baltimore County, Baltimore, MD, USA

Correspondence: Yuxuan Wang (ywang246@central.uh.edu)

Abstract. Coastal regions are susceptible to multiple complex dynamic and chemical mechanisms and emission sources that lead to frequently observed large tropospheric ozone variations. These large ozone variations occur on a meso-scale which have proven to be arduous to simulate using chemical transport models (CTMs). We present a clustering analysis of multi-dimensional measurements from ozone Light Detection And Ranging (LiDAR) in conjunction with both an offline GEOS-Chem CTM simulation and the online GEOS-Chem simulation GEOS-CF, to investigate the vertical and temporal variability of coastal ozone during three recent air quality campaigns: 2017 Ozone Water-Land Environmental Transition Study (OWLETS)-1, 2018 OWLETS-2, and 2018 Long Island Sound Tropospheric Ozone Study (LISTOS). We developed and tested a clustering method that resulted in 5 ozone profile curtain clusters. The established 5 clusters all varied significantly in ozone magnitude vertically and temporally which allowed us to characterize the coastal ozone behavior. The lidar clusters provided a simplified way to evaluate the two CTMs for their performance of diverse coastal ozone cases. An overall evaluation of the models reveals good agreement ($R \approx 0.70$) in the low-level altitude range (0 to 2000 m), with a low and unsystematic bias for GEOS-Chem and high systemic positive bias for GEOS-CF. The mid-level (2000 – 4000 m) performances show a high systematic negative bias for GEOS-Chem and an overall low unsystematic bias for GEOS-CF and a generally weak agreement to the lidar observations ($R = 0.12$ and 0.22, respectively). In evaluating the cluster specific performances additional model insight is revealed as cluster-by-cluster model performance is more convoluted than the overall performances suggest. Utilizing the full vertical and diurnal ozone distribution information specific to lidar measurements, this work provides new insights on model's proficiency in complex coastal regions.

1. Introduction

Tropospheric ozone (O_3) is an important secondary pollutant created by multiple reactions involving sunlight, nitrogen oxides (NO_x = NO + NO_2), and volatile organic compounds (VOCs) which, in accumulation, can have damaging effects on human and plant health. In addition to its photochemical growth, O_3 can easily be influenced by local and regional transport mechanisms. For coastal regions, surface O_3 is highly variable in time and space due to its susceptibility to many factors such as local ship emissions, long range transport, and sea/bay breeze processes. Multiple studies have proven the strong influence that sea/bay breeze and wind flow patterns can have on the accumulation of coastal O_3 and can often lead to poor air quality (e.g., Tucker et al., 2010; Martins et al., 2012; Stauffer et al., 2012; Li et al., 2020). Loughner et al. (2014) highlighted the importance for understanding the ability for bay breeze events to cause O_3 differences not only spatially but vertically in coastal regions.

This variability is challenging for air quality models to capture as high-resolution measurements are necessary to fully understand and simulate this O_3 behavior in coastal regions. For example, Dreessen et al. (2019) tested the U.S. Environmental Protection Agency (EPA) Community Multiscale Air Quality (CMAQ) model's ability, configured at 12 km, to simulate O_3 exceedances at Hart Miller Island in Maryland (HMI) revealing high bias and 'false alarms' due to several reasons such as emission transport over water and the coarse model resolution's inability to capture fine-scale meteorology and transport. Cases such as sea/bay breeze events, which directly contribute to high coastal O_3 cases, are denoted by local meteorological mechanisms such as surface wind speed deceleration, wind direction convergence and recirculation (Banta et al., 2005). Air quality models with coarse horizontal and vertical resolutions are not able to capture such fine developments (Caicedo et al., 2019). Ring et al. (2018) also used CMAQ to estimate the impact of ship emissions on the air quality in eastern U.S. coastal regions indicating that an understanding of the vertical profiles of emissions was significant for improving air quality simulations. These are consistent and unanimous issues with air quality modeling in coastal regions. Since offshore sites within coastal regions are historically under sampled due to the difficulty of water-based measurements, this problem is still pertinent today.

Recently, three associated air quality campaigns set out to address this issue (https://www-air.larc.nasa.gov/index.html): 2017 & 2018 NASA Ozone Water-Land Environmental Transition Study (OWLETS-1 & OWLETS-2) and Long Island Sound Tropospheric Ozone Study (LISTOS) (e.g., Sullivan et al., 2019). These three campaigns were each conducted in highly populated coastal regions along the Chesapeake Bay in Virginia and Maryland and Long Island Sound in the New England/Middle Atlantic region, respectively, that are vulnerable to O_3 exceedances with the goal of filling the measurement gaps in these regions. During these campaigns, a suite of detailed airborne and ground measurements were taken during the course of highly polluted summer months (end of May through August) to capture the variability of pollutants, including O_3 and its precursor species, and the distinct meteorological processes specific to land-water regions that affect them.

The three campaigns strategically placed multi-dimensional tropospheric lidar measurements of O_3 on and offshore in order to capture critical land-water gradients and to fill the deficit of measurements in these under monitored areas. These measurements were supported as part of NASA's Tropospheric Ozone Lidar Network (TOLNet). Continuous profile

measurements from O_3 lidars highlight important regional transport and temporal variations of O_3 in the lower and middle levels of the troposphere that are usually difficult to capture by most satellite-based remote-sensing instruments (Thompson et al., 2014). Lidar measurements are unique in their ability to capture high resolution full O_3 2-D profile curtains over a period of time that indicate pollutant transport and can help in understanding O_3 behavior in coastal regions. In Gronoff et al. (2019), the co-located lidar at the Chesapeake Bay Tunnel Bridge (CBBT) during OWLETS-1 successfully captured a near-surface maritime ship plume emission event on August 01, 2017. An ensemble of other instruments (e.g., drones, Pandora spectrometer systems, etc.) launched near the shipping channel captured elevated NO_2 concentrations while the lidar instrument captured a depletion of O_3 simultaneously. The lidar was able to capture the unique low range altitude O_3 concentrations which elucidated the evolution of the trace-gas concentrations during this ship plume event.

Several studies have thoroughly evaluated the results from the air quality campaigns used in this study but were focused more on specific case studies (Dacic et al., 2019; Sullivan et al., 2019; Gronoff et al., 2019). Dacic et al. (2019) used lidar measurements of a high O_3 episode during OWLETS-1 to evaluate the ability of two NASA coupled chemistry-meteorology models (CCMMs), the GEOS Composition Forecast ("GEOS-CF"; Keller et al., 2021) and MERRA2-GMI (Strode et al., 2019), to simulate this high O_3 event. They found that the GEOS-CF model performed fairly in simulating O_3 in the lower level (between 400 to 2000 m ASL) and outperformed MERRA2-GMI based on surface observations at multiple monitoring sites and by a median difference of -6 to 8 % +/- 7 % at both lidar sites. In the case of this event, GEOS-CF was able to simulate the 2-D O_3 profile curtains at small scales. At the time of the Dacic et al. (2019) study, only processed observational data from OWLETS-1 was available.

For this study, we took advantage of 91 captured 2-D (vertical and diurnal) O_3 profile curtains from all three air quality campaigns (Sect. 2). To characterize the different behaviors of O_3 in coastal regions, we developed a novel clustering method based on the altitude and time dimensions of the lidar measurements that organized the profile curtains (Sect. 2). We used the developed clusters to evaluate the ability of both offline and online GEOS-Chem and GEOS-CF simulations to reproduce the coastal O_3 and wind characteristics highlighted by each cluster (Sect. 3).

2. Materials & Method

2.1. Air quality campaigns

During the years 2017 and 2018, NASA in partnership with other U.S. national agencies and university research groups orchestrated three air quality campaign studies that focused on key land and water observations: OWLETS-1, OWLETS-2, and LISTOS. OWLETS-1 was conducted in 2017 from July 5 to August 3, while OWLETS-2 and LISTOS were conducted in 2018 from June 6 to July 6 and July 12 to August 29, respectively. All campaigns took advantage of a multitude of ground, aircraft, and remote sensing measurements. For the sake of this study, we will focus on measurements from the two lidars from the TOLNet: NASA Langley Mobile Ozone Lidar (LMOL) (De Young et al. 2017; Farris et al. 2018; Gronoff et al, 2019, 2021) and NASA Goddard Space Flight Center (GSFC) Tropospheric Ozone (TROPOZ) Differential Absorption Lidar (DIAL) (Sullivan et al. 2014, 2015a), which ran simultaneously at the marked positions in Figure 1. The TOLNet data from all three

campaigns are available on the NASA LaRC Airborne Science Data for Atmospheric Composition archive (https://www-air.larc.nasa.gov/missions.htm; accessed – 20 January 2021).

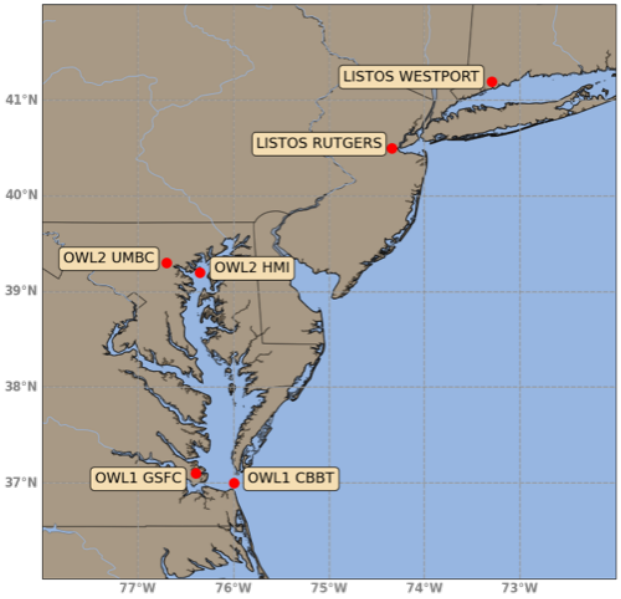

Figure 1. An inset map of the Chesapeake Bay airshed in Maryland, Virginia, and Long Island Sound in New York with the six lidar monitoring locations used for OWLETS-1, OWLETS-2, and LISTOS highlighted and labeled.

The two lidars were placed strategically for each campaign (Figure 1), so that one lidar was closest to over-water measurements while the other was farther inland with the goal of examining how O_3 transport and concentration is influenced by specific coastal mechanisms such as the land–water breezes. For OWLETS-1, the LMOL lidar was used at the CBBT [37.0366°N, 76.0767°W], depicting the real time over water O_3 measurements while the GSFC TROPOZ lidar was stationed at NASA Langley Center [37.1024°N, 76.3929°W] further inland. Similarly, for OWLETS-2, the LMOL lidar was stationed for the over water measurements at Hart Miller Island [39.2449° N, 76.3583° W] and GSFC TROPOZ was stationed at the University of Maryland, Baltimore County (UMBC) [39.2557° N, 76.7111° W]. Finally, for LISTOS, LMOL was at the Westport site [41.1415° N, 73.3579° W] and TROPOZ at Rutgers [40.2823° N, 74.2525° W]. For the sake of this study the unique benefits due to the different placements (onshore versus offshore) of the co-located lidars are not specifically evaluated. Instead, the study focuses on the benefits of detailed and multi-dimensionality of both lidar instrument data in general.

Routine lidar measurements were taken for the duration of the campaigns providing 91 multi-dimensional O_3 profile curtains. Both lidars retrieve data at a 5-min temporal resolution and use a common processing scheme to produce a final O_3 product which was used for this study. In this study, the individual profile curtains refer to the "full day", vertical and diurnal

lidar measurements. In this study, 91 individual 2-D profile curtains were used from both lidars from the three campaigns: 26 profile curtains from OWLETS-1, 28 profile curtains from OWLETS-2, and 37 profile curtains from LISTOS.

To evaluate meteorological impacts on the lidar O_3 clusters and distinguish certain model discrepancies we used various temperature and wind measurements. Hourly observed temperature, wind speed and wind direction, and O_3 from surface monitors pertaining to the study area were obtained from the Air Quality System (AQS) (data can be accessed at https://aqs.epa.gov/aqsweb/airdata/). Along with the O_3 lidar instruments, we utilized high resolution vertical and horizontal wind speed and direction data monitored by Doppler wind lidar Leosphere WINDCUBE 200s instruments deployed at HMI during OWLETS-2 during LISTOS (e.g., Couillard et al., 2021; Coggon et al., 2021; Wu et al., 2021).

2.2. Clustering lidar data

2.2.1 Description of the ozone lidar measurements

The lidar instrument is unique in that it provides high dimensional profile measurements of O_3, as opposed to one dimensional surface measurements from air quality monitoring sites. The two TOLNet lidars used during the campaigns have been evaluated for their accuracy during previous air quality campaigns (DISCOVER-AQ; https://www-air.larc.nasa.gov/missions/discover-aq and FRAPPÉ; https://www2.acom.ucar.edu/frappe) and have also been compared against each other (e.g., Sullivan et al., 2015; Wang et al., 2017). The two lidars have different transmitter and retrieval components but produce O_3 profiles within 10 % of each other as well as compared to ozonesondes (Sullivan et al., 2015). In comparison with other in situ instrument measurements, the TOLNet lidars were found to have an accuracy better than ±15 % for capturing high temporal tropospheric O_3 vertically proving their capability of capturing high temporal tropospheric O_3 variability (Wang et al., 2017; Leblanc et al., 2018).

To characterize coastal O_3 during the summer months, we use a multitude of lidar profile curtains obtained during the OWLETS-1, 2, and LISTOS campaigns. The two lidars used in the campaigns produced profile curtains of O_3 from 0 – 6000 m above ground level (AGL) with some days beginning as early as 06:00 local time (EDT) and ending measurements as late as the last hour of the day. One of the challenges is that the multiple lidar datasets are not always uniform; although most of the profile curtains began at or around 08:00 EDT, the lidar measurements commence and conclude at different times. At the time of these campaigns, the lidar data retrieval was constrained by the availability of personnel as well as the availability of electricity in remote areas (at time of writing, the lidar instrument systems have been updated and are now more fully automatized for use during succeeding campaigns removing such constraints). Due to this constraint, the 91 lidar curtains range from as short as a 6-hour window to a full 24-hour window. Similarly, the profile curtains do not have an exact uniform altitude range either. In the processing of the lidar data, some measurements may be filtered out and removed due to issues, such as clouds, which can influence and degrade the retrieval leaving some blocks of empty data within the vertical altitude dimension. When the cloud conditions are perfect, the limiting factor for the altitude is the solar background: the UV from the sun is a source of noise that prevents the detection of the low level of backscattered photons. For LMOL, this means that the maximum altitude is about 10 km AGL at night (Gronoff et al., 2021) and lowered to about 4 km AGL at solar noon (worse

conditions possible for the summer in the continental U.S. resulting in below 4 km AGL). This results in a general scarcity of O_3 measurements above 4000 m AGL for most of the vertical profile curtains. Lidars still have limitations that prove to be a complication e.g., noise signal and manual operations. At the time of writing, the operative limitation has been addressed and the lidars are now more fully automated which removes some of the difficulty.

2.2.2 Clustering approach and application

To facilitate the comparison of the 2-D O_3 profile curtains and the air quality model simulations we used a cluster analysis that categorized the behavior of the tropospheric O_3 captured in the profile curtains. Clustering methods are commonly used in air quality and atmospheric studies to group and characterize large datasets (Darby, 2005; Alonso et al., 2006; Christiansen, 2007; Davis et al., 2010; Stauffer et al., 2018). In our previous work, we have successfully used clustering methods to automatically characterize diurnal patterns of surface winds and surface O_3 in the Houston-Galveston-Brazoria area that proved to perform better than a rudimentary quantile method to reveal the dependence of surface O_3 variability on local and synoptic circulation patterns on the Gulf Coast (Bernier et al., 2019; Li et al., 2020)

In evaluating the structure of the lidar measurements and working within measurement limitations (described in Sect. 2.2.1) from the three air quality campaigns, we developed a method to cluster multi-dimensional O_3 profile curtains using K-Means clustering algorithm. Input features (seed values) were rationally established to best represent the behavior of O_3 temporally and vertically without including an excessive amount of input features, which can weaken the results of clustering (discussed in detail in Sect. S1). With the goal of evaluating lower level tropospheric O_3 and based on description of the structure and constraints of the lidar measurements, the features were tailored to the altitude range 0 – 4000 m AGL and time range of 06:00 EDT – 21:00 EDT.

Figure 2 illustrates the 8 features that represent slabs of altitude and time used in the cluster analysis. For each O_3 profile curtain (total of 91), we calculated the average O_3 from the following time and altitude range: Features 1 – 4 altitudes range from 0 – 2000 m; Features 5 – 8 altitudes range from 2000 – 4000 m. The two altitude ranges were determined to best represent different O_3 transport events although they do not explicitly represent these layers. For Features 1 – 4, O_3 would most likely primarily be affected by local production and pollution transport while for Features 5 – 8, O_3 would more likely be associated with long range transport (e.g. interstate). As planetary boundary layer growth (PBL) in coastal regions do not usually reach altitudes greater than 2000 m, mixing between the boundary layer and free troposphere would presumably take place within the low-level altitude bin. Additional attention to the PBL in the selecting of low versus mid-level features for the clustering will be investigated in future work. For clarity, we will use the terms low-level and mid-level features to address the two altitude subsets e.g., Features 1 – 4 and 5 – 8, respectively. Feature 1 and 5 time range from 06:00 – 08:00 EDT; Feature 2 and 6 from 08:00 – 12:00 EDT; Feature 3 and 7 from 12:00 – 16:00 EDT; and Feature 4 and 8 from 16:00 – 21:00 EDT. The four subset time ranges were indicated to best represent features that characterize the common diurnal behavior of O_3.

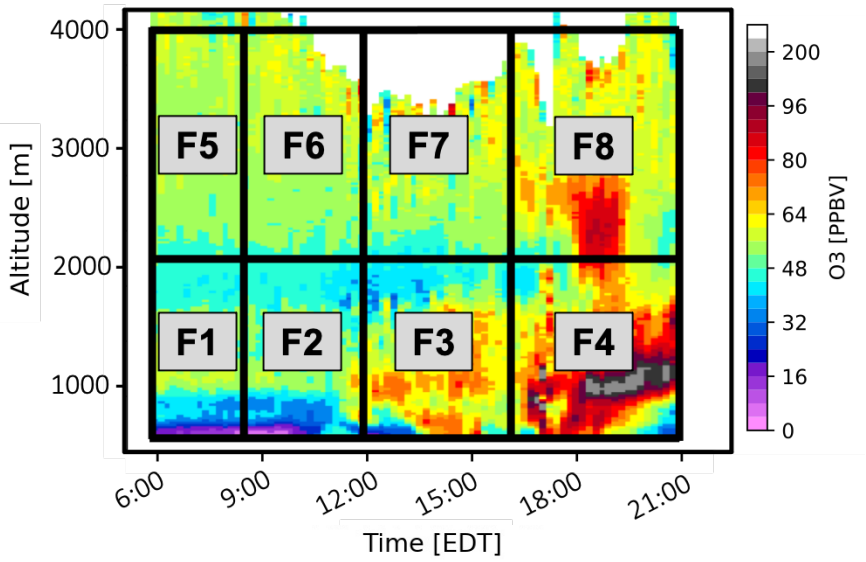

Figure 2. Clustering method developed for clustering vertical O_3 profiles taken from lidar measurements. The color coding shows a typical day of lidar measurements of O_3 profiles on August 6, 2018, from the LMOL at Westport, CT during the LISTOS Campaign. F1 – F8 indicate the time and altitude range of the eight features used for the clustering algorithm.

The features were evaluated for cluster tendency, essentially to confirm our dataset contained meaningful clusters (discussed in detail in Sect. S2). One statistical approach was used to test the dataset called Hopkins statistic which measures whether there is uniform distribution (spatial randomness) within the dataset (Lawson and Jurs, 1990). The results calculated using the Hopkins statistic concluded a value higher than 0.75 (actual = 0.77) which by this standard indicates a clustering tendency at the 90 % confidence level. Evaluating different feature options did not lead to better statistical results than with the final chosen features. To visualize the cluster tendency of our dataset, we applied the algorithm of the visual assessment of cluster tendency (VAT) approach (Bezdek and Hathaway, 2002) which uses the Euclidean distance measure to compute the dissimilarity matrix in the dataset and creates an ordered dissimilarity matrix image. Figure S1 shows the VAT approach results which indicates high similarity (red) and low similarity (blue) and confirms a cluster structure (not random) within our dataset.

Since the choice of clustering algorithm is subjective, we chose K-means clustering for its simplicity and widespread use. To use the K-Means clustering algorithm, the optimal number of clusters based on your dataset must be chosen beforehand. For this study, the package Nbclust (Charrad et al., 2014) in R was used, which applies 30 indices for determining the optimal number of clusters. Using this package, as well as testing the quality of the clustering results using the silhouette method (Kaufman & Rousseeuw, 1990), we selected six clusters as the optimal number of clusters. Since the K-Means clustering algorithm is based on the Euclidean distance to each centroid, the input data was normalized (to a mean of zero and standard deviation of one) to ensure each feature is given the same importance in the clustering (Aksoy & Haralick, 2001; Larose,

2005). The resulting six clusters (described fully in Sect. 3.1) represent clusters of regularly observed lidar O_3 curtains for the regions of our study during the campaign periods.

2.2.3 Missing data

Although the input features were tailored based on the structure of the lidar measurements, the remaining data still had missing data points. In performing a quick evaluation on the 8 input features (Figure S5), we found that Features 1, 4, 5, and 8 had the most missing data while Features 2, 3, 6, and 7 had few or zero cases of missing data. This means that the earlier morning measurements (06:00 – 12:00 EDT) and the later evening measurements (16:00 – 21:00 EDT) had the most cases of missing data points. This is plausible as the campaign teams were best able to retrieve clear measurement during midday/evening hours (12:00 – 16:00 EDT). As a result, 51 out of 91 O_3 profile curtains had at least one missing data point (feature) throughout the individual profile curtain.

A common practice for dealing with missing data is complete case analysis (CCA), in which observations with missing values are completely ignored, leaving only the complete data to cluster. CCA can be inefficient as it introduces selection bias since the sample data no longer retains the state of the original full dataset (Donders et al., 2006; Little & Rubin, 2014). When we applied CCA, there were only 40 O_3 profile curtains of complete data, removing over half of the study profiles. Instead, we used a more comprehensive solution – imputation - that yields unbiased results (Donders et al., 2006). For this study we used the single imputation (SI) technique *knnImputation* in R (Torgo, 2010), which uses the k-nearest neighbors and searches for the most similar cases and uses the weighted average of the values of those neighbors to fill the missing data. Essentially, this method selects the days that have the most similar profile curtain to any profile which has missing data points and uses those real data points to calculate a weighted mean that will fill in the missing data. We acknowledge using an imputation method on the dataset will possibly introduce a bias which is difficult to quantify, but this allows the use of the full 91 profile curtains of O_3 data. The silhouette method was used to test the quality of the newly imputed dataset and proved to be no worse, nor better, than the CCA (*real data*) results. Therefore, the dataset was first imputed using SI to create a complete dataset and then the clustering method described in the sect. before (2.2.2) was applied to the complete imputed dataset.

2.3. Model simulations

The offline GEOS-Chem chemical-transport model (CTM) was utilized to simulate the spatial and temporal variability of coastal O_3 in the Chesapeake Bay and Long Island Sound during the time of the campaigns. The GEOS-Chem model is a global 3-D CTM driven by assimilated meteorological data from the NASA Global Modeling and Assimilation Office (GMAO). Our simulations were driven by reanalysis data from Modern-Era Retrospective analysis for Research and Applications, Version 2 (MERRA-2; Gelaro et al., 2017). We ran a nested GEOS-Chem (v12-09) simulation at 0.5° x 0.625° horizontal resolution over the eastern portion of North America and adjacent ocean (90 – 60°W, 20 – 50°N), using lateral boundary conditions updated every three hours from a global simulation with 2° x 2.5° horizontal resolution. The nested GEOS-Chem simulation was run with 72 vertical levels from 1013 to 0.01 hPa. Since the study focuses on the altitude range

0 – 4000 m, the first 20 vertical levels from GEOS-Chem were used with 14 levels within the boundary layer (≤ 2000 m). The nested simulation was conducted for the study periods June – September 2017 and April – August 2018. We used the standard "out-of-the-box" unmodified default settings from the tropospheric chemistry chemical mechanism (tropchem) with global anthropogenic emissions from the Community Emissions Data System (CEDS) inventory (McDuffie et al, 2020) and U.S. Environmental Protection Agency (EPA) National Emissions Inventory (NEI) 2011 for monthly mean North American regional emissions (EPA NEI, 2015).

We also used results from NASA's near real-time forecasting system, GEOS-CF, an online GEOS-Chem simulation (v12-0-1) from GMAO (https://gmao.gsfc.nasa.gov/-weather_prediction/GEOS-CF/) with GEOS coupled to the GEOS-Chem tropospheric-stratospheric unified chemistry extension (UCX) and run at a high spatial resolution of 0.25°, roughly 25 km (Keller et al., 2021, Knowland et al., 2021). The vertical resolution for GEOS-CF is interpolated onto 72 vertical levels from 1000 to 10 hPa. Since the study focuses on the altitude range 0 – 4000 m, the first 21 vertical levels from GEOS-CF were used with 14 levels within the boundary layer (≤ 2000 m). Prior to the launch of the 12z five-day forecast, GEOS-CF produces daily global, 3-D atmospheric composition distributions using the GEOS meteorological replay technique (Orbe et al., 2017), and this study makes use of these historical estimates, made available to the public for the period since January 2018. Therefore, the GEOS-CF results shown in this study only include the dates from OWLETS-2 and LISTOS campaigns, since they both occurred in 2018.

While both model simulations use similar versions of GEOS-Chem chemistry, there are noteworthy differences to keep in mind during the analysis of the clustering. The main differences between the two models are (1) GEOS-Chem is an offline CTM using archived meteorology, while GEOS-CF simulates atmospheric composition simultaneously with meteorology (online); (2) the spatial resolution of the GEOS-CF model (0.25°) is higher than GEOS-Chem (0.5° x 0.625°); and (3) the GEOS-CF model runs with Harmonized Gridded Air Pollution (HTAP; v2.2; base year 2010) anthropogenic emissions from the Emission Database for Global Atmospheric Research (EDGAR), while GEOS-Chem was run with CEDS anthropogenic emissions (base year 2014). These imperative differences can lead to disparities in the following results.

3. Results & Discussion

3.1 Overview of the 2-D O_3 curtain clusters

The clustering results reveal distinctive characterized O_3 behavior during the three campaigns in which O_3 concentrations vary across the clusters. As previously mentioned in Sect. 2.2.3, the clustering analysis initially identified six cluster groups from the O_3 profile curtains. Only one date was assigned to Cluster 6 (16 June 2018): the lidar profile curtain on this day (Figure S6) shows a large fraction of data missing, and the available data have relatively high O_3 throughout the lowest 3 km, which is different from other clusters. Therefore, we consider Cluster 6 to be an outlier and will not include it in the subsequent analysis.

Various O_3 and surface meteorological parameter cluster statistics for the remaining five clusters are summarized in Table 1. With only 5 of the 2-D profile curtains assigned, Cluster 5 depicts the least common O_3 behavior during the campaigns. On

the other hand, Cluster 3 is the most common O_3 behavior during the campaigns with 28 profile curtains assigned to this cluster. Following Cluster 3, Cluster 1 is the next most common cluster with 25 profile curtains. Cluster 2 and Cluster 4 fall in the middle with 14 and 18 profile curtains assigned to the cluster numbers, respectively.

Cluster #	**a) No. of vertical profiles**	**b) O_3 Max** (ppb)	**c) O_3 Min** (ppb)	**d) T avg.** (min; max) (°F)	**e) WS avg.** (min; max) (m s^{-1})
1	25	86.5	42.2	74.1 (67.8; 86.4)	1.5 (0.5; 2.8)
2	14	72.8	28.9	71.6 (64.0; 83.9)	1.6 (0.6; 2.9)
3	28	86.6	34.2	77.2 (67.0; 87.6)	1.3 (0.5; 2.4)
4	18	97.8	44.1	78.4 (68.0; 90.4)	1.2 (0.4; 2.3)
5	5	67.7	29.1	74.5 (66.8; 74.5)	1.2 (0.3; 3.4)

Table 1. Lidar vertical O_3 profile cluster statistics: a) total number of vertical profiles; b) O_3 maximum; c) O_3 minimum O_3;) AQS monitoring station cluster mean d) surface temperature and e) wind speed; minimum and maximums in parenthesis. The statistics and averages were derived from the total number of profile curtains assigned to each cluster.

The five clusters were distinguished by the varying O_3 concentrations between the low-level and mid-level as well as diurnal variations (Figure 3). Figure 3a quantifies the between-cluster differences. We separate the data by the two altitude subsets (low and mid-level) and by two time subsets (morning = 6:00 – 12:00 and afternoon = 12:00 – 21:00) for lucidity as the majority of the cluster differences are contrasted between these subsets. In the low-level, all five clusters exhibit the common O_3 diurnal pattern where surface O_3 is titrated overnight and reaches a minimum but then is quickly exacerbated with the increase of sunlight throughout the day and typically peaks after midday (Figure 3b). The extent of this common diurnal pattern varies by cluster.

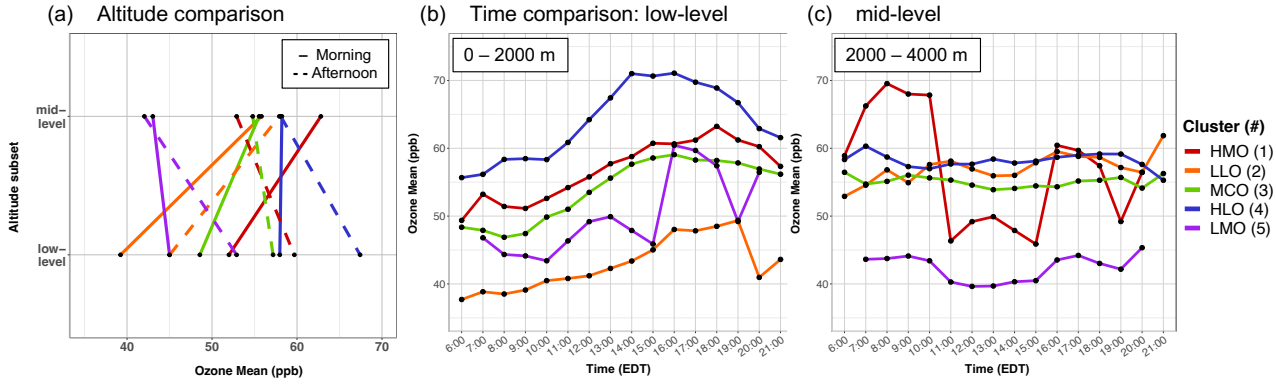

Figure 3. Lidar O_3 cluster average comparisons (five clusters depicted in colors). a) Altitude comparison of mean O_3 averaged over time: morning hours from 6:00 – 12:00 (solid line) and afternoon hours from 12:00 – 21:00 (dashed lines). Time comparison of mean hourly O_3 split between the b) low-level and c) mid-level.

Cluster 1 in the low-level has the second highest morning and afternoon O_3 average (52 and 59 ppb) and in the mid-level the highest morning O_3 average (64 ppb) (Figure 3a). Cluster 1 also exhibits the most unique pattern of mid-level O_3 (Figure 3c), with the highest concentrations found in the early morning and an uncharacteristic plunge to lower O_3 concentrations from 11:00 – 15:00 EDT. This is contrary to the other clusters which do not show much O_3 variation temporally in the mid-level. The majority of the individual profile curtains assigned to Cluster 1 show concentrated early morning residual layers in the mid-level that diffuse after the morning, which is distinctive to the other clusters. In the low-level, Cluster 2 has the lowest morning and afternoon O_3 average among the clusters (39 and 45 ppb) with moderate mid-level O_3 concentrations. Cluster 3 has the most uniform vertical O_3 extent between the low and mid-level (Figure 3a), in contrast to the other clusters that differ greatly in O_3 concentrations between the two altitude subsets. Cluster 4 has the highest morning and afternoon O_3 averages (59 and 68 ppb) in the low-level, reaching > 70 ppb temporally (Figure 3b). Finally, Cluster 5 has, considerably, the lowest morning and afternoon O_3 averages (42 and 43 ppb) in the mid-level, almost 10 ppb lower than the other clusters. Cluster 5 does not have a smooth-evolving O_3 diurnal pattern in the lower level (Figure 3b), which can be attributed to the averaging of only five different profile curtains that were assigned to this cluster (Table 1).

Figure 4a illustrates the mean lidar O_3 2-D profile curtains for each of the clusters. For Cluster 1, 3, 4, and 5, higher O_3 concentrations in the low-level are captured during afternoon/evening time (12:00 – 21:00 EDT), with the highest low-level O_3 in Cluster 4 (> 70 ppb). This behavior follows the common diurnal pattern of O_3, that was distinguishable in Figure 3b. This common O_3 growth reaches vertically to approximately 1500 m for each of the clusters but is generally contained below 2000 m. Differing from the low-level O_3 behavior, mid-level O_3 is generally less variable in magnitude throughout the entire profile curtain (except for Cluster 1; see Figure 3a). The highest O_3 concentrations for the mid-level are exhibited in Cluster 1, 2, 3, and 4, with the highest mid-level O_3 in Cluster 1 during the early morning hours (≥ 70 ppb).

Following the descriptions above, each cluster is given a nomenclature according to their unique characteristics. Cluster 1 is termed as the highest mid-level O_3 (HMO) cluster; Cluster 2 as the lowest low-level O_3 (LLO) cluster; Cluster 3 is the most common O_3 (MCO) cluster; Cluster 4 is the highest low-level O_3 (HLO); Cluster 5 is the least common and lowest mid-level O_3 (LMO) cluster. The O_3 variability represented and justified above is what led to the successful clustering of the lidar O_3 2-D profile curtains.

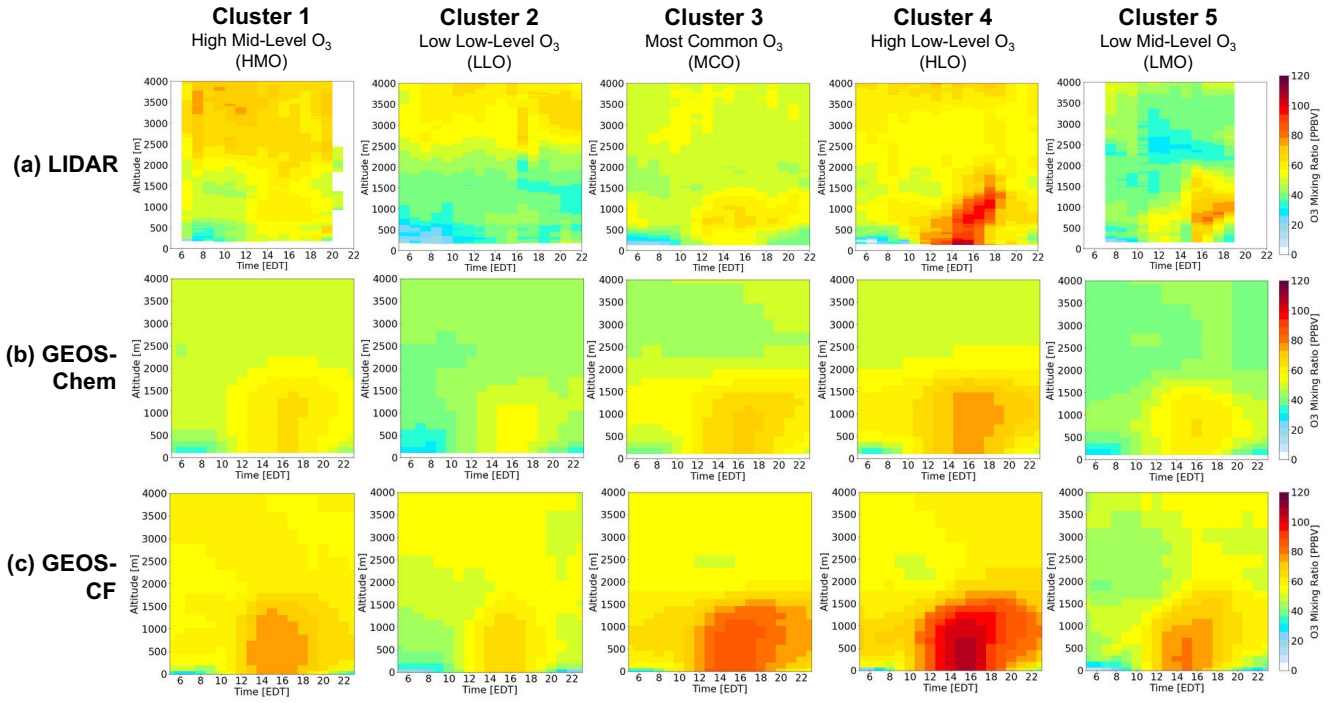

Figure 4. Cluster-mean O_3 vertical profile results by cluster assignment (1- 5) and arranged: a) LIDAR; b) GEOS-Chem simulation; and c) GEOS-CF simulation.

The clustering analysis results provided a characterization of O_3 behavior that transpired during these three campaigns. Figure 3b and 3c indicate each cluster represents a different O_3 evolution pattern, likely related to different photochemical or transport regimes. This kind of evaluation is useful in that it combines O_3 information from both temporal and vertical dimensions. For example, the HLO cluster reveals the specific case in which higher O_3 is captured early in the temporal profile in the low-level and translates to the higher O_3 captured in the low-level as well. The profile curtains show higher background O_3, indicating these cases did not have "clean air" to begin with which can allow a greater accumulation in the low-level in the afternoon. This is an example of how this type of clustering analysis, if applied, could demonstrate background O_3 in the similar case studies. In another example, several profile curtains assigned to the HMO cluster indicate concentrated residual layers in the mid-level and possible entrainment to the surface as the day progressed. To prove this feature, vertical velocity and vertical velocity variance data would be needed but the knowledge that a clustering approach is able to pinpoint these features that could only be discernible through lidar measurements proves to be useful. The clustering results was valuable in recognizing a significant large pollution related cluster (HLO), a total of 18 out of the 91 curtain profiles which correspond with the highest daily surface maxima measured at these sites (= 97.77 ppb) (Table 1). This cluster, on average, exhibited a daily surface maxima up to 10 ppb greater than any of the other clusters. Discerning these higher O_3 cases is imperative for mitigating severe air pollution.

3.2. Cluster surface analysis

To support the lidar clustering results, daily averaged meteorological surface observations from AQS stations pertaining to the campaign period and GEOS-Chem surface model output were evaluated in regard to the five clusters. Figure 5 shows the cluster mean surface temperature from AQS stations and GEOS-Chem model as well as the simulated wind speed and direction. The average surface temperature from each station is represented as the circular markers while the simulated temperatures are represented as the spatial contour and the simulated wind speed (m s^{-1}) and direction as arrows. Cluster average, minimum, and maximum AQS surface temperature and wind speed can be found in Table 1d, e.

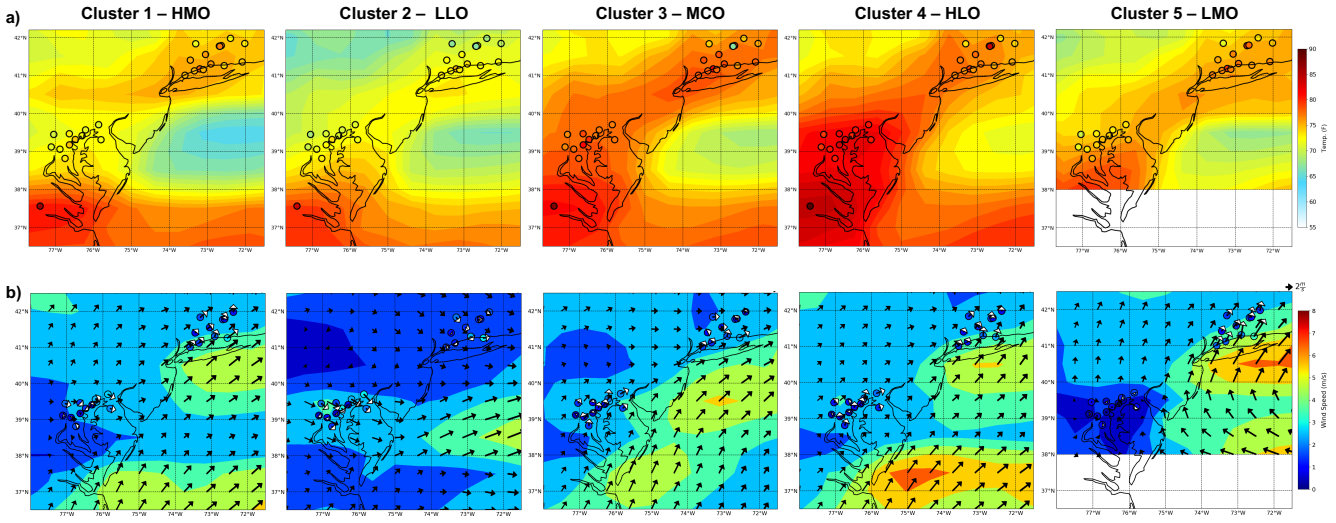

Figure 5. Cluster averaged meteorological surface AQS station observations and GEOS-Chem model results. a) Surface temperature observations represented as the circular markers and simulated surface temperatures represented as the spatial contour (top-panel). b) Surface wind speed and direction observations represented as the circular markers and white arrows and simulated wind speed and direction represented as spatial contour and black arrows (bottom-panel).

In general, the surface meteorological conditions agree with our knowledge of transport and O_3 production that would lead to each of the five clustered lidar O_3 profile curtains. It is evident that the clusters with the highest surface O_3 (HMO, MCO, and HLO) all share a predominant offshore, westerly wind. Furthermore, MCO and HLO presented higher overall observed and simulated surface temperatures compared to the other clusters (Figure 5a). Observed and simulated wind speeds reveal slightly lower average wind speeds and primarily continental wind flow for both clusters as well (Figure 5b). These meteorological conditions are conducive to a higher production of surface O_3 concentrations which validates the higher O_3 found in the low-level results (Figure 3b, 4a).

Conversely, the lowest surface temperatures are found in LLO. Lower surface temperatures are also indicative of low vertical mixing due to less generation of convection. Relatively calm wind speeds and lower temperatures indicate other possible meteorological factors such as high cloud cover that could have contributed to the lower O_3 concentrations in LLO. Although surface O_3 concentrations in LMO reach higher levels later in the day, first at 13:00 EDT and then again at 16:00 EDT, the rest of the temporal profile stays below moderate levels. Average temperatures for LMO are moderately high but, in contrast, the average wind speed is higher (specifically over the Long Island Sound) and unique to the other clusters, wind direction is predominantly onshore (Easterly – Southerly). This prevalent onshore flow indicates a transport of cleaner marine air which corroborates the lower surface O_3 levels. LMO did not have any profile curtains assigned from OWLETS-1 which is why data for the lower Chesapeake Bay area is not shown in Figure 5.

There was only one occurrence during the dates in which the lidar instruments were operating in which there was a recorded maximum daily 8-hour average (MDA8) O_3 exceedance (> 70 ppbv). This exceedance date is 25 May 2018 in which 3 AQS sites in the LISTOS region measured MDA8 O_3 of 73, 72, and 72 ppbv. This curtain profile was assigned to the HMO cluster (Cluster 1), the cluster with high O_3 in the mid-level and moderate O_3 in the low-level and near the surface.

3.3. Evaluating the GEOS-Chem and GEOS-CF model

In this sect. the model results from GEOS-Chem and GEOS-CF will be compared to the lidar data using the five lidar O_3 profile clusters discussed in Sect. 3.1. Both model results were sampled in an equal manner, in which we extracted the same cluster date assignments from the lidar clusters and created mean vertical profiles based on the model results. This allowed us to evaluate the model performance based on the five characterized O_3 lidar clusters. As mentioned previously, the GEOS-CF simulation data is not available for 2017. Thus, the results shown subsequently will only include GEOS-CF results from 2018 (only dates from the OWLETS-2 and LISTOS campaigns). The GEOS-Chem simulation results include both years thus all three campaign duration periods.

3.3.1 Overall model performance

Figure 4b and 4c depict the simulated cluster-mean O_3 profile curtains from GEOS-Chem and GEOS-CF, mirroring the mean lidar profile curtains in Figure 4a. For all clusters in the low-level, both models simulate a consistent accumulation of O_3 near the surface after 12:00 EDT, mirroring the O_3 common diurnal pattern depicted in mean lidar profile curtains in Figure 4a. However, the extent the models simulate is often higher in magnitude than the observations, specifically GEOS-CF consistently predicting the accumulation at a higher magnitude than GEOS-Chem. In the mid-level, both models simulate much less O_3 variability than what is captured in the lidar observations. Figure 4b and 4c clearly show how the models struggle to reproduce any mid-level O_3 pattern or variability that is relayed in the lidar observations. This is in contrast to the low-level where the models are able to reproduce the common diurnal pattern of O_3. With the lidar data providing a full temporal and vertical profile curtain of O_3 behavior and development, we are able to indicate areas where the models struggle such as in this case in the mid-level.

We first evaluate overall correlation and biases between the model and lidar data. The overall correlation between both models and the lidar data, disregarding the specific clusters, based on the two altitude subsets as the performances differ between low-level and mid-level for both GEOS-Chem (Figure S7a) and GEOS-CF (Figure S7b). The mean normalized biases for the five clusters displayed in Table S1 (in Supplementary Material) were calculated from the total vertical and diurnal averages separated by low-level and mid-level. For both models, overall low-level O_3 correlation rounds to 0.70, signifying a strong relationship between the model simulations and the lidar observations (Figure S7 - top panel). This indicates that both models can simulate the development and pattern of O_3 well in the low-level. Overall, GEOS-Chem performs well in simulating low-level O_3 with a lower non-systematic normalized bias ranging from -0.10 to +0.13 for the five clusters. Thus, based on the lower bias, GEOS-Chem fairs well simulating the magnitude of low-level O_3 as well. For all clusters, GEOS-CF overestimates the average magnitude of low-level O_3 with a systematic high positive normalized bias ranging from +0.30 to +0.67. This consistently high bias reveals that GEOS-CF generally is unable to simulate low-level O_3 magnitude well.

For the mid-level, the overall correlation reveals that GEOS-CF and GEOS-Chem both have a weak relationship with the lidar (R = 0.22 and R = 0.12, respectively) (Figure S7 - bottom panel). This indicates that neither model is able to simulate mid-level O_3 pattern well. GEOS-Chem consistently underestimates the magnitude of mid-level O_3 with a systematic high negative normalized bias ranging from -0.44 to -0.18, for all clusters, while GEOS-CF has a lower and non-systematic normalized bias ranging from -0.22 to 0.28. Overall, both models are not able to simulate the variability of O_3 nor the magnitude well in the mid-level. The overall analysis in this sect. provides a fundamental but condensed assessment of model performance. In the next sect., the cluster specific differences reveal additional model performance insight that would be conceivably overlooked when evaluating overall performance.

3.3.2 Model evaluation based on lidar clusters

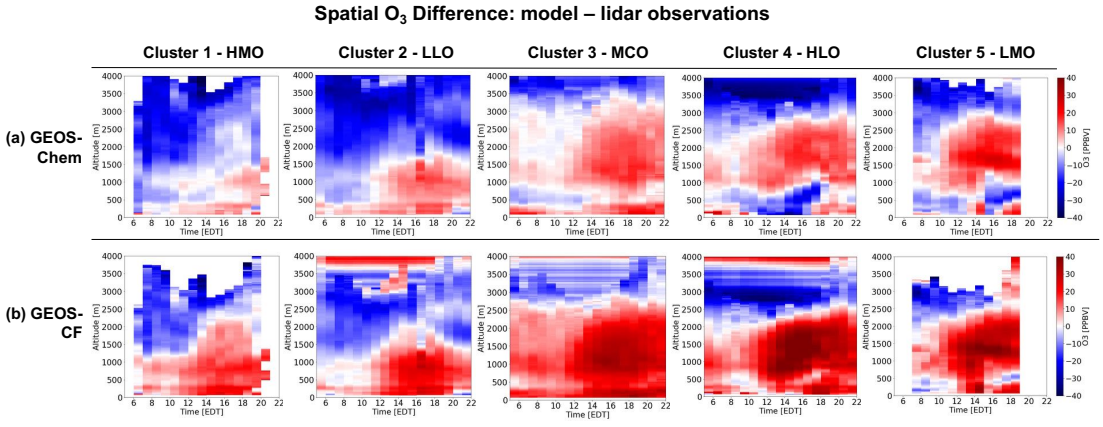

Figure 6. Mean profile curtain spatial O_3 difference (model – lidar observations) for each cluster (1 – 5). GEOS-Chem differences (a) and GEOS-CF differences (b).

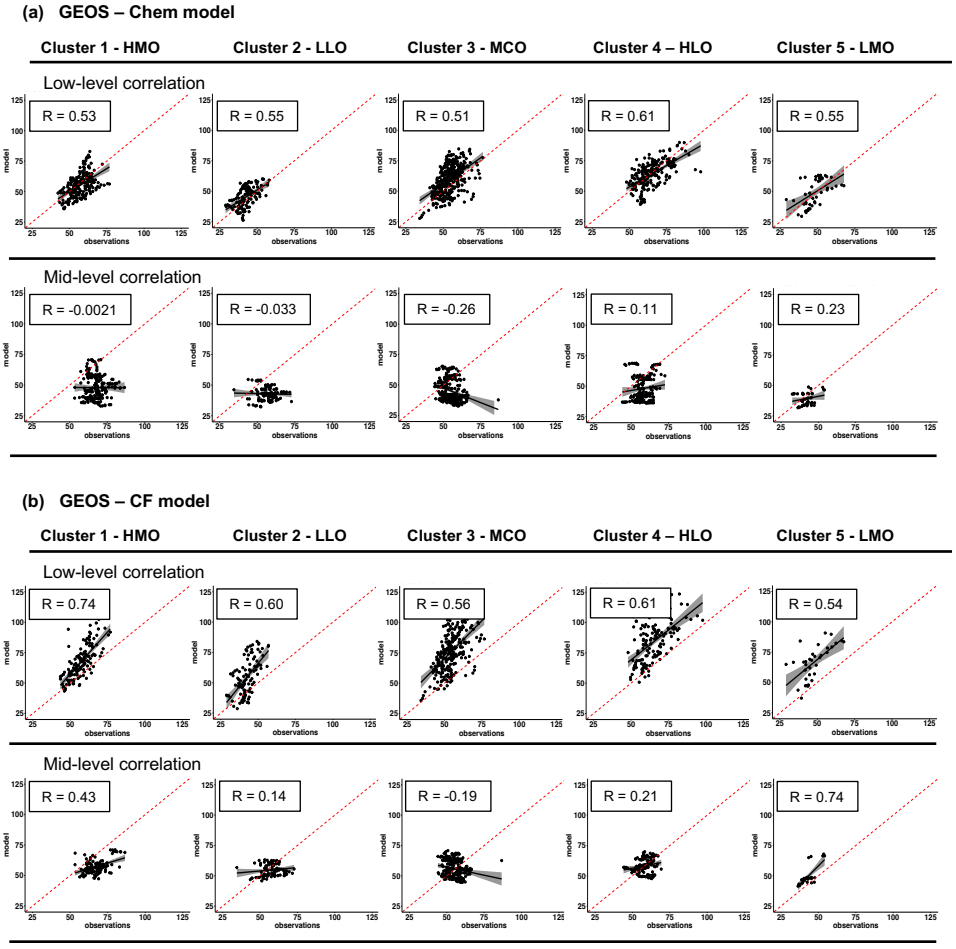

Figure 7. O_3 correlation between lidar observations and a) GEOS-Chem model simulation results and b) GEOS-CF model results by each cluster split by low-level (top panel) and mid-level (bottom panel).

Significant cluster by cluster differences are unmasked in evaluating the models based on the established O_3 behavior cases. To quantify the results illustrated in Figure 4, we show spatial O_3 differences (model – lidar observations) for each cluster (Figure 6) as well as individual cluster correlation (Figure 7) (subsequent cluster calculated normalized biases and correlation can be found in Table S1). Evaluating the individual cluster biases and correlation reveal more in-depth model discrepancies as well as areas where the models perform well.

In the low-level, GEOS-CF has a similar performance ability for the HMO, HLO, and LMO clusters with high positive biases at + 0.30, + 0.41, and + 0.45 respectively. These higher biases imply GEOS-CF has difficulty capturing moderate O_3 concentrations below 2000 m (HMO and LMO) as well as the in the high O_3 cases (HLO). GEOS-CF also has a high positive bias (+ 0.50) in the LLO cluster indicating that GEOS-CF struggles to capture the lower O_3 concentrations in the low-level.

This is warranted as models are intended to approximate and are not usually able to capture extremes (high or low) but GEOS-CF also seems to struggle capturing moderate cases as well. In the low-level, GEOS-Chem has the best performance (minimal -0.04 bias and strong correlation, R = 0.61) in HLO, which is the cluster with the highest low-level O_3 accumulation (refer to Figure 4a). The second-best performance for GEOS-Chem in the low-level follows closely behind (minimal +0.07 bias and fair correlation, R = 0.55) in LLO, the cluster with the lowest O_3 accumulation. These results suggest GEOS-Chem actually performs well in cases of high O_3 as well as cases of low O_3 with a slight tendency to overpredict lower O_3 concentrations and underpredict higher O_3 concentrations. This challenges the overall assumption that models struggle to capture extreme cases since GEOS-Chem actually performs best in simulating both extreme cases of high O_3 in HLO and, again, low O_3 in LLO. GEOS-Chem has a similar performance for the LMO and HMO clusters with negative biases of – 0.10 and – 0.09, respectively. GEOS-Chem is also able to capture the moderate O_3 in both of these clusters well with slight underestimations.

Both models perform the worst (in comparison with the other clusters) in the low-level in the MCO cluster with a + 0.13 bias for GEOS-Chem and + 0.67 bias for GEOS-CF. As described in Sect. 3.1, MCO is the most common cluster with moderate - high average O_3 concentrations in the low-level (refer to Figure 3b). Although GEOS-Chem has the worst performance in the MCO cluster, it is not necessarily a poor performance. The performance follows the conclusion previously made that GEOS-Chem can fairly simulate moderate O_3 in the low-level although, in this case, with slight overestimations. Contrarily, the GEOS-CF performance in the MCO cluster reveals a more substantially high positive bias. This stands out as models are usually able to capture moderate levels (e.g., non-extreme cases). Evaluating the full temporal and vertical profile indicates that the higher GEOS-CF bias in the MCO cluster is additionally influenced by the greater overestimation of morning O_3, not solely the afternoon O_3. This is different to the performance in the LLO and LMO clusters where GEOS-CF also had a high positive bias in the low-level but does better simulating the early morning O_3 magnitude. A similar conclusion can be drawn when evaluating the low-level GEOS-Chem performance. HMO, LLO, MCO, and LMO all share 'higher' biases (rounding to +/– 0.10), but the highest bias is found in the MCO cluster. Analogous to GEOS-CF, this can similarly be attributed to GEOS-Chem overestimating morning O_3 the worst in the MCO cluster in contrast to the better early morning estimation in the other clusters.

In the mid-level, GEOS-Chem underestimates O_3 magnitude to the greatest extent in the HMO and the LLO cluster (both bias = – 0.44), which are both clusters with higher mid-level O_3 concentrations (refer to Figure 3c). GEOS-Chem performs similarly in the HLO and MCO clusters, with a negative mean bias of – 0.30 and – 0.27, respectively. This indicates that GEOS-Chem most struggles to simulate higher concentrations of O_3 in the mid-level. The GEOS-Chem model actually never reaches O_3 cluster averages greater than 50 ppb, directly divulging the greater systemic negative bias in the mid-level. GEOS-Chem simulates LMO mid-level O_3 magnitude the best (– 0.18 bias), which is the cluster with the lowest O_3 average (< 45 ppb). Although for the LMO cluster GEOS-Chem has a lower bias, the correlation is still poor (R = 0.23) which indicates that the model is relatively capable of simulating mid-level O_3 only when the case devises lower concentrations but still fails to replicate any O_3 variability and pattern.

On the other hand, GEOS-CF does best simulating LLO, MCO, and HLO, which are all clusters with moderate O_3 in the mid-level (≥ 50 and ≤ 70 ppb). GEOS-CF has the highest bias in the LMO cluster (+ 0.28), the cluster with the lowest mid-level O_3 magnitude. GEOS-CF also has the strongest correlation in the same LMO cluster (R = 0.74). This is a unique case where although GEOS-CF is not able to capture the magnitude in the mid-level, it is able to capture the pattern of low O_3 well. Comparing the full multi-dimensional lidar and model mean profile curtains it is evident that in the LMO cluster, the GEOS-CF model simulates a similar mid-level O_3 pattern in the early morning/afternoon that is captured in the mean lidar curtain profile. The second worst performance for GEOS-CF is the underestimation of mid-level O_3 in the HMO cluster, contrarily the cluster with the highest mid-level O_3 (≥ 70 ppb). This supports the previous conclusion that although GEOS-CF has a relatively lower biases in the mid-level, the model still struggles to simulate the extreme O_3 cases. Although GEOS-CF underestimates O_3 magnitude in the HMO cluster, it actually has a higher correlation than most of the other clusters (R = 0.43) (Figure 7, Table S1). In comparing the full multi-dimensional lidar and model mean profile curtain (Figure 3), GEOS-CF does a fair job connecting the mid-level higher O_3 pattern in the early morning that develops down to the low-level later in the afternoon. From this we can draw a conclusion that GEOS-CF is better able to capture mid-level O_3 patterns earlier in the temporal profile leading to higher correlations with the lidar.

3.3.3 Cluster approach and model conclusions

Several studies rely on case study investigations or grouping data by altitude to evaluate model performance. As demonstrated in Sect. 3.3.1, we can evaluate the overall summarized the model profile curtains O_3 against the lidar profile curtains and come to the simple conclusion that both models fairly simulate low-level O_3 but struggle to simulate mid-level O_3. However, a systematic and comprehensive understanding of the different photochemical regimes in coastal regions does not only require case studies and overall summaries. The clustering approach allows for a comprehensive yet still detailed evaluation of the different photochemical regimes in coastal regions utilizing the lidar derived full profile curtains. Additionally, using the clusters, we can efficiently evaluate the ability of the models to simulate many different cases of O_3. This approach revealed specific O_3 cases in which the models perform well and others where the models fail that would have been overlooked by solely considering the overall results. Using the clustering, we are able evaluate how the cluster specific differences (Figure 6, Figure 7, and Table S1) reveal additional model performance insight and specific gaps that would be conceivably overlooked when evaluating overall performance.

It is warranted that models struggle simulating extreme events/cases such as seen in the low-level in the HLO cluster and in the LLO cluster. However, GEOS-Chem performs best in both clusters with minimal biases and strong to fair correlations. Our result suggest that GEOS-Chem does a much better job simulating extreme O_3 cases in the low-level than expected. This specific model feature is not eminent when evaluating overall performance. Additionally, overall GEOS-Chem performs poorly in the mid-level. The detailed analysis granted by the cluster approach reveals GEOS-Chem has the lowest bias in the LMO cluster signifying the model is better able to capture low O_3 conditions in the mid-level. The overall high systemic positive bias for GEOS-CF in the low-level is further dissected when evaluating the individual clusters. GEOS-CF

systematically overestimates low-level O_3, but the individual clusters indicate that the model has a better correlation with O_3 in HMO cases. An even more profound case is exposed in which GEOS-CF has a strong correlation with mid-level O_3 in the LMO cases despite having a low correlation overall. This concludes that in cases where the GEOS-CF model struggles to reproduce O_3 concentrations, the model can still capture the O_3 variability seen by the lidar measurements.

The clustering approach also reveals more discrepancies in the models such as in the MCO cluster. The advantage of evaluating full temporal and vertical profile curtains indicates that overestimation of early morning O_3 throughout the low-level leads to the poorer performances in MCO for both models. The overestimation of morning O_3 in GEOS-CF adds to the systemic overestimation in afternoon O_3 contributing the greater bias and poorer correlation. The same case can be found in the GEOS-Chem MCO cluster performance but to a lesser extent as GEOS-Chem has a much lower positive bias. Previous studies have found that excessive vertical mixing leads to overestimation of O_3 near the surface as well as underestimation of O_3 night-time depletion resulting in overestimation of O_3 the next day (Dacic et al., 2020; Keller et al., 2021; Travis & Jacob, 2019). The titration that occurs at night after the initial afternoon build up requires successful simulation to prevent the model beginning the following day with higher O_3 than is observed which can lead to the overprediction of O_3 later that day. Therefore, in the given case where there is an O_3 event that lasts more than one day (at the same lidar location), the model will likely underestimate O_3 night-time depletion, overpredict morning O_3, and subsequently overpredict the afternoon build-up. Given multiple cases of multi-day high O_3 events from the lidar measurements (17 total from HMO, MCO, and HLO), this is likely one of the reasons for GEOS-CF overestimating early and therefore afternoon O_3 in these high O_3 cases in the low-level. In Figure 6, GEOS-CF exhibits the greatest afternoon O_3 overprediction in MCO and HLO. In HLO alone, there were 4 (out of 18) of the profiles that were consecutive while in MCO there were 8 (out of 28). This gives explanation for upwards of 22 – 29 % of the overestimation of O_3 in the profile curtains of these clusters. These multi-day O_3 events are particularly important as they can indubitably lead the models to higher overprediction of afternoon O_3. As the full lidar profile curtains reveal, the models tend to overestimate early morning O_3 in the MCO cases which links to the overestimation in afternoon O_3 as well.

Both models have a better ability to simulate early morning O_3 magnitude and pattern for other clusters than the MCO. For example, GEOS-CF does best simulating morning low-level O_3 in cases of lower O_3 extent (LLO and LMO). Excluding MCO, GEOS-Chem does not have such an issue overestimating low-level O_3 in the afternoon. In the other clusters, GEOS-Chem actually underpredicts early morning low-level O_3 in the full vertical profile. An underestimation of early morning O_3 does not warrant the same build-up up of afternoon O_3. This gives some explanation to why GEOS-Chem underpredicts the other clusters with higher O_3 concentrations in the low-level (HMO and HLO). In the mid-level GEOS-Chem has a systemic high negative bias for all clusters, consistently underestimating O_3 but the clusters reveal a better performance in LMO, the cluster with lowest mid-level O_3 extent. It is evident that the model cannot simulate cases with higher O_3 concentrations in the mid-level but simulates low O_3 cases better. On the other hand, GEOS-CF results indicate a lower non-systemic bias in the mid-level. Since the version of GEOS-Chem used in this study was run with the tropchem chemistry mechanism which excludes stratospheric chemistry (now obsolete with current GEOS-Chem developments) and GEOS-CF uses the UCX chemistry mechanism that includes stratospheric chemistry, this may allude to better performance of GEOS-CF in simulating

higher O_3 concentrations in the mid-level. Both models indicate weak correlations with the lidar observations in the mid-level and it is apparent that both models struggle to capture the pattern of O_3 behavior in the mid-level. This could be due to multiple model inefficiencies such as the coarse model resolutions. Although GEOS-CF has a finer resolution than GEOS-Chem, it still may not be sufficient in horizontal and vertical grid resolution to replicate the O_3 variations captured in the 2-D lidar observations.

There are additional model discrepancies that can lead to underestimations of O_3 in GEOS-Chem in the mid-level that was found in all 5 clusters. One gap in the GEOS-Chem model could be the representation of tropospheric halogen chemistry which has a large effect of coastal O_3 production. Newer updates to the GEOS-Chem model (v12.9) have included updated tropospheric halogen chemistry mechanisms (iodine, bromine, and chlorine) (Wang et al., 2021). This study found that the updated halogen chemistry actually worsens the overall underestimation of O_3 throughout the troposphere, specifically in the northern hemisphere, indicating further investigation of halogen chemistry is needed for better model representation. Another study finds a similar conclusion in the proper representation of cloud uptake and tropospheric chemistry (Holmes et al., 2019). This study found that implementing an updated, more accurate, and stable cloud entrainment-limited uptake in the GEOS-Chem model reduces the sensitivity of oxidants and aerosol chemistry in the troposphere but still had little effect on O_3 model comparison to observations (such as sonde and aircraft). This is due to the environmental variability being much higher than the effect of NO_x and O_3 cloud chemistry but still warrants further testing. The role lightning plays in tropospheric oxidation is another feature that is commonly misrepresented in global models and can affect O_3 simulation (Mao et al., 2021). These are all examples of features that if not simulated correctly can lead to misestimations of O_3. The clustering approach allows us to organize the detailed lidar measurements to scope out specific cases where these misrepresentations occur. These previous studies also highlight the importance of lidar measurements and their ability to depict tropospheric emission development and behavior throughout the vertical profile and diurnal cycle which can be used to constrain model emissions and improve simulations.

Although this analysis proves to be a useful technique to characterize the largely variably O_3 behavior in coastal regions and evaluate the subsequent model performance, there are also limitations. In this study we are comparing single point lidar versus model output, therefore we cannot simply state that the model is incorrect. We make conclusions and draw biases based on the ability to subset a grid point and compare that to a single point lidar curtain to the best ability but that still leaves an uncertainty. The high vertical and spatiotemporal resolution reveal intricate details about the behavior of O_3 during these campaigns. O_3 lidars have a unique advantage, compared to traditional surface measurements, in measuring vertical distribution of O_3 with respect to time. This advantage is of great value when investigating model ability in simulating the spatial and temporal distribution of O_3 and can provide crucial information in understanding surface O_3 events.

3.4 Cluster derived case studies to evaluate modeled wind and ozone

Meteorological factors such as wind speed and direction can directly impact whether a coastal region will experience clean air or O_3 exceedances. When local meteorological processes such as sea/bay breeze occur at such a fine scale, equally

fine resolution measurements are essential in capturing this. The Doppler wind lidar offers a focus on fine details that are only revealed in the multi-dimensional data which allows for such a comprehensive evaluation of the established O_3 cluster profile curtains. In this sect., we evaluate the 2-D relationship between wind and O_3 to assess model performance using lidar and model derived profile curtains (Figure 8). We derived two specific case studies, each from a different cluster: MCO = 17 June 2018 and HLO = 30 June 2018. Utilizing the derived clusters, the case studies were chosen to focus on high low-level O_3 behavior cases with a goal of evaluating possible sea/bay breeze events. The two case studies are both from the HMI location during the OWLETS-2 campaign. There are consistent Doppler lidar measurements throughout the low-level (< 2000 m) which allows for a direct comparison with the simulated profiles; therefore, the focus of the following analysis will be on the low-level altitudes. The deficit of mid-level observed wind data disallows for a conclusive and concrete evaluation of simulated mid-level O_3.

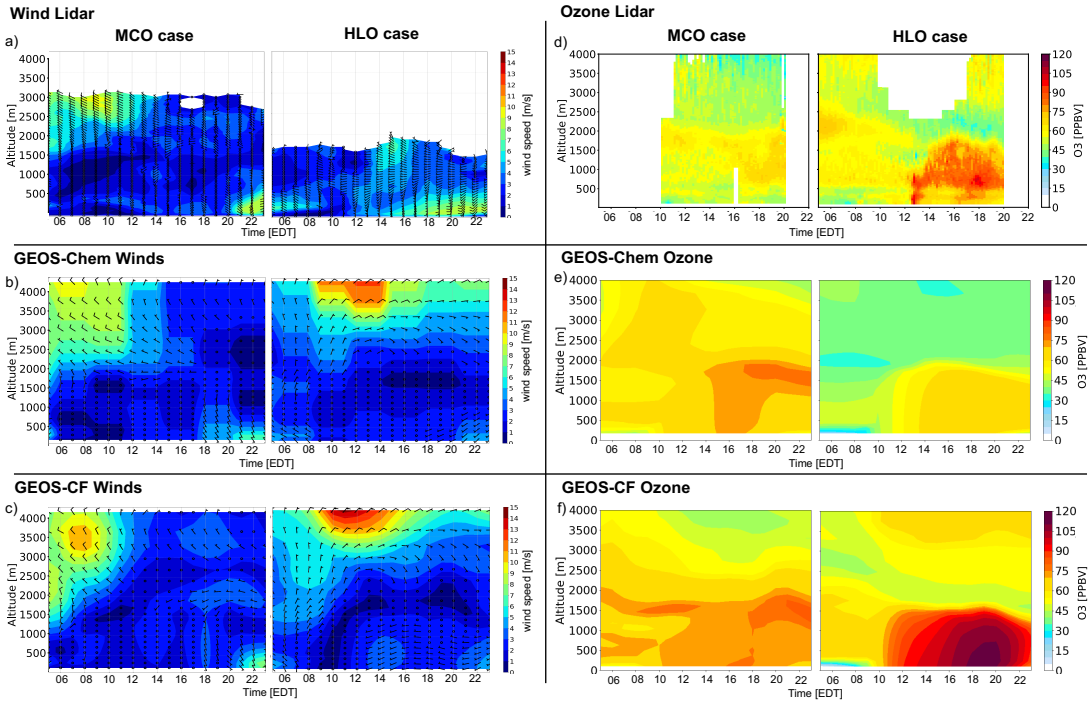

Figure 8. Profile curtains of wind speed/direction (a-c) and ozone (d-f) from the lidar (top panel), GEOS-Chem (middle panel), and GEOS-CF (bottom panel). Results from OWLETS-2 at HMI.

3.4.1 Sea breeze event interpretation

GEOS-Chem and GEOS-CF both struggle to capture low-level wind speed and direction in both MCO and HLO cases (Figure 8a-c). In the MCO case, the Doppler wind lidar captures a wind direction shift from westerly to easterly winds beginning at 06:00 EDT accompanied by calm winds (approximately 0 m s^{-1}) indicating a likely common sea/bay breeze event. The timing of the start of this event is simulated well but the models fail to predict an actual well-defined wind shift, instead

merely simulating 0 m s^{-1} winds after 05:00 EDT. It is apparent that the models struggle to capture the finer processes such as a sea/bay breeze which could have likely led the underprediction of wind speed. It is important to note that GEOS-Chem runs with offline meteorology, averaged every 3 hours. Since sea/bay breezes often happen at a finer temporal resolution, the GEOS-Chem model is at a disadvantage in modelling such fine processes. A wind direction shift is also depicted in the HLO case, with westerly winds early in the morning and a shift to south-easterly winds later in the temporal profile (at about 10:00 EDT). This could also likely be an early onset sea breeze event which could have contributed to the high observed O_3 concentrations in the afternoon. Again, the exact timing of the start of the wind shift is captured by the models but then no defined directional shift and little to no winds are simulated after. Both the MCO case and HLO case observe increased wind speeds near the surface, first before 08:00 EDT then again in the evening. Both models underestimate the extent of the increased wind speeds.

3.4.2 Relation to ozone cases and clustering

In this sect., the wind lidar curtains will be assessed in relation to the O_3 lidar profile curtains and the model performance. The results in sect. 3 revealed that both models had the highest bias and lowest correlation simulating low-level O_3 in MCO. Evaluating the wind and O_3 lidar profile curtains against the model simulations helps paint a better picture as to why. Similar to the MCO cluster mean curtain profile, early morning low-level O_3 in each case is overestimated by both models (Figure 8e, f). There is higher O_3 captured in the lidar curtain profile, but it is constrained between 1500 – 2000 m. Both models bring this higher O_3 pattern down to the surface (below 500 m) overestimating O_3 throughout the low-level. Since both models predict little to no winds during this time, this could contribute to overestimations of O_3 near the surface.

In the HLO case, GEOS-CF overestimates low-level O_3 while GEOS-Chem underestimates low-level O_3. From sect. 3.3 the results revealed that although GEOS-CF has a high positive normalized bias for low-level O_3 in HLO, the model had a reasonable relationship ($R = 0.61$) with the O_3 lidar measurements. This is corroborated with the individual HLO case (Figure 8f) as GEOS-CF is better able to simulate the development of O_3 in the low-level, especially in the early morning. The GEOS-CF modeled winds mirror this performance with a better reproduction of the wind shift in HLO (Figure 8c). While GEOS-Chem has a lower normalized bias for low-level O_3 in the HLO cluster, GEOS-Chem consistently underestimates wind speed and fails to reproduce any wind shifts. This reveals that in the possible sea breeze event, the two models do not perform equally. Since GEOS-Chem is an offline CTM using archived meteorology and GEOS-CF simulates atmospheric composition simultaneously with meteorology (online), the replication of a sea breeze case would not necessarily be comparable.

In most cases, sea/bay breeze events can contribute to high concentrated daytime O_3 events in which O_3 is recirculated throughout the region. Such cases would likely lead to a similar curtain profile as seen in the HLO case (Figure 8a), where high O_3 in the morning is likely associated with the higher O_3 at the surface in the afternoon. But it is apparent that the cases for MCO and HLO are dissimilar. We would expect per the clustering approach that sea breeze cases would most likely be assigned to the same cluster, but this is not the case here. Investigating the full lidar and model profile curtains for the two cases gives us more information as to why these two curtains are not in the same cluster. It is evident that the HLO case has much higher afternoon O_3 near the surface (below 1000 m) than the MCO case, with peaks > 75 ppb at both 12:00 and again

at 16:00 EDT. In contrast, the MCO case has higher afternoon O_3 concentrations captured above 2000 m than the HLO case. The HLO case has high O_3 in the afternoon, but it is constrained to the lower 2000 m and just above this high O_3 plume, there is an O_3 deficit of almost 50 ppb. Although the MCO case also reveals lower O_3 above 2000 m, the vertical gradient in this case is not as stark. This is also replicated in both models which simulate lower O_3 directly above the high surface O_3 in the HLO cluster but simulate much higher O_3 above 2000 m in the MCO cluster. From their distinct vertical and temporal behavior, it is easy to conclude why these two cases were not assigned to the same cluster.

The cases elected for MCO and HLO give reason to address the difficulty simulating complex coastal mechanisms. Despite the fact that MCO and HLO both indicated prospective sea/bay breeze cases, the results of the simulated winds and O_3 were distinctive. Simulating complex sea/bay and land relations is imperative for correctly mitigating high O_3 cases. To accurately simulate such complex exchanges, high resolution vertical and horizontal simulations are needed. Because of the models' relatively coarse resolutions (nominally 50 and 25 km horizonal resolution; 72 vertical levels), the fine-scale vertical wind gradients and horizontal wind shifts are difficult to resolve and, in these cases, not fully able to replicate. This study also acknowledges the need for an evaluation of other modeled factors, such as divulged in sect. 3.3.3, considering the possible confounding effects on modeled O_3 outcome.

4. Conclusion

We developed and tested a clustering method on a suite of 91 multi-dimensional lidar O_3 profile curtains retrieved from three recent land/sea campaigns (OWLETS-1, OWLETS-2, and LISTOS), during the summer months of 2017 and 2018. The K-Means clustering algorithm, driven by 8 well defined features, was applied to categorize the fine resolution O_3 data, revealing five distinct O_3 behavior cases that are distinct in pattern and magnitude vertically and temporally. We present five different clusters of O_3 behavior identified as: highest mid-level O_3 (HMO) cluster; lowest low-level O_3 (LLO) cluster; most common O_3 (MCO) cluster; highest low-level O_3 (HLO); lowest mid-level O_3 (LMO) cluster. The results indicate that fine resolution data can be used to differentiate the behavior of O_3 in a region and classify different cases of O_3 exploiting the multiple dimensions. The clustering approach allowed us to characterize the range of highly variable vertical and temporal coastal O_3 behavior for the duration of these campaigns which can be a good indicator of how O_3 behaves in general in these coastal regions during the summer months. Furthermore, this approach could be used by states to better identify different O_3 photochemical regimes and frequency beyond just surface sampling.

We evaluated the performance of two CTMs, GEOS-Chem and GEOS-CF, in these complex environments. Overall, the models have the greatest difficulty simulating the vertical extent and variability of O_3 concentrations in the mid-level, with weak overall relationships to the lidar observations ($R = 0.12$ and 0.22). GEOS-Chem had a systematic high negative bias and GEOS-CF an overall lower unsystematic bias range. In the low-level, GEOS-Chem had overall low unsystematic bias range and fair relationship with the lidar observations ($R = 0.66$), while GEOS-CF had a systematic high positive bias but overall fair relationship ($R = 0.69$).

Utilizing the curated clusters reveals new model insight that is neglected in the overall performance analysis. The cluster approach divulges specific model limitations but also cases in which the models perform well. GEOS-Chem simulates low-level O_3 cases best in the HLO and LLO clusters and the worst in the MCO cluster. HLO and LLO are the clusters with the most extreme (low and high) O_3 cases while MCO is the most common cluster with moderate O_3. This concludes that GEOS-Chem does best simulating extreme low-level O_3 but struggles to capture the frequently occurring moderate O_3 behavior. GEOS-CF also has the greatest overestimations for low-level O_3 in the MCO cluster. Evaluating the full profile curtain reveals that this overestimation can be most attributed to the greater overestimation of early morning O_3. This feature is unique to the MCO cluster and warrants further investigation as O_3 left in the residual layer can contribute to higher O_3 in the afternoon and proves to be a challenge for CTMs. The value of lidar measurements is reflected in its ability to reveal these features.

Both models share poor performances in the mid-level but there are specific cases that stand out in the clustering results, specifically the LMO cluster, in which GEOS-CF shares a good agreement with the lidar measurements. It can be concluded that although the model struggles to simulate O_3 magnitude, it can relatively emulate the mid-level O_3 pattern in LMO. This is also apparent in the MCO cluster, in which the pattern of higher mid-level O_3 that suggests a relationship with the low-level O_3 is simulated fairly in the GEOS-CF model. This pattern is also a rare feature that is captured in the lidar that demonstrates the significance of the measurements. The greater underestimations of mid-level O_3 for GEOS-Chem can be alluded to multiple model discrepancies. Since the GEOS-Chem version and mechanism used in this study (tropchem) only considers tropospheric chemistry we can expect the performance in the mid-level to have deficiencies. Although GEOS-CF is run with the combined tropospheric and stratospheric chemistry mechanism, has a better grid resolution, and is an online model, there are still limitations to both models especially when simulating mid-level O_3. Known model errors and coarse horizontal and vertical grid resolution contribute to the difficulty in simulating fine-scale coastal O_3 variability. There are many contributing model factors that can be affecting the performance of GEOS-Chem and GEOS-CF that were mentioned in this study not solely coarse model resolution.

A unique value of the clustering approach on multi-dimensional lidar data is that it offers a convenient way to ascertain different O_3 case studies. An example of this is our evaluation of two cases studies from the MCO and HLO clusters. Modeled winds were evaluated using Doppler wind lidar data observed during the OWLETS-2 campaign. The wind lidar data was mostly limited to lower altitudes (< 2000 m), which allowed for wind speed and direction validation at the low-level. The morning wind deceleration and directional shifts (onshore to offshore) illustrated in lidar profile curtains indicate a possible sea/bay breeze event in both case studies. This is likely another contributor that led to enhanced surface O_3 in these cases. Due to the coarser model resolution, GEOS-Chem and GEOS-CF were not able to capture the sea breeze phenomena in these cases which could have facilitated in the high O_3 biases for these clusters. With GEOS-CF having a finer horizontal resolution than GEOS-Chem, the results reveal minimal advantages simulating the pattern of wind speeds better but none in simulating the wind directional shifts. This affirms that the spatial resolution of GEOS-CF (~25 km) is still not fine enough for mesoscale processes such as the sea/bay breeze. Although a regional model analysis is out of the scope of this study, we propose to use

multi-dimensional lidar measurements to evaluate finer regional modeling in our future work. We acknowledge that other factors, aside from model resolution, contribute to discrepancies in modeled coastal O_3 and further warrant a deeper evaluation. The clustering approach on lidar measurements offers an unmatched ability to pinpoint these features.

This work is the first time that all three associated campaign lidar data have been analyzed in conjunction. In utilizing the highly detailed suite of multi-dimensional lidar data, we are able to comprehensively explore the behavior and variability of coastal O_3 for the duration of the campaigns. Applying the clustering analysis directly to the lidar O_3 data emerges as a useful and robust approach for identifying O_3 patterns during the highly polluted summer months in coastal environments. Since the time of the OWLETS and LISTOS campaigns, the lidar instrument systems have been updated and are now more fully automatized for use eliminating such constraints faced in this study. Further observations using lidar instruments should be especially valuable in investigating coastal O_3 behavior as it can divulge the finer-scale O_3 characteristics that remain difficult to successfully simulate in CTMs. The time-height and fine resolution measurements only available from multi-dimensional lidar instruments were vital in allowing us to form these conclusions.

This kind of evaluation allows for detailed model assessment of specific O_3 cases that are unmasked through the clustering analysis. Looking at the overall correlations, it would seem the models have a good relationship with the low-level lidar observations but looking into the cluster-by-cluster differences, the gaps within the models are elucidated. Using the cluster assignments, we are able evaluate how the cluster specific differences reveal additional model performance insight that could be conceivably overlooked when evaluating overall performance. This work is a middle ground between looking at specific cases (or dates) and summarizing overall model performance. Additionally, the clustering approach provides an abridged way to detecting distinctive case studies. We provide a new approach that allows a synopsis of summer coastal O_3 behavior and subsequently model performance without completely muting distinct O_3 features. Evaluating model performance for diverse O_3 behavior in coastal regions is crucial for improving the simulation and furthermore, mitigation of air quality events.

Code availability. Model code is available upon request to the first author.

Data availability. The GEOS-Chem model simulation data from this study is publicly accessible online at https://doi.org/10.7910/DVN/V99LHT. The GEOS-CF model data is publicly available online at their website https://gmao.gsfc.nasa.gov/-weather_prediction/GEOS-CF/. The lidar data is publicly available online at https://www-air.larc.nasa.gov/missions.htm.

Supplement.

Author contributions. CB and YW conceived the research idea. CB wrote the initial draft of the paper and performed the analyses and model development. All authors contributed to the interpretation of the results and the preparation of the paper.

Competing interests. The authors declare that they have no conflict of interest.

Acknowledgements. This study is supported by NASA MUREP Graduate Fellowship (80NSSC19K1680). The Ozone Water-Land Environmental Transition Study (OWLETS-1, 2) and Long Island Sound Tropospheric Ozone Study (LISTOS) field measurements described here were funded by the NASA's Tropospheric Composition Program and Science Innovation Fund (SIF), Maryland Department of Environment, the National Oceanic and Atmospheric Administration (NOAA), the Environmental Protection Agency (EPA), the Northeast States for Coordinated Air Use Management (NESCAUM), and the New Jersey and Connecticut Departments of Energy and Environmental Protection. The authors acknowledge the principal investigators and data operators John Sullivan, Joel Dreessen, Ruben Delgado, William Carrion, and Joseph Sparrow as well as the guidance of the Tropospheric Ozone Lidar Network (TOLNet). LMOL and TROPOZ data are publicly available at (https://www-air.larc.nasa.gov/missions/TOLNet/). The OWLETS and LISTOS data are available at (https://www-air.larc.nasa.gov/). The Doppler wind data taken from the UMBC wind lidar and are publicly available at (https://www-air.larc.nasa.gov/cgi-bin/ArcView/owlets.2018). The GEOS-CF model simulation data were provided directly from the NASA Center Global Modeling and Assimilation Office (GMAO) at the Goddard Space Flight Center (https://gmao.gsfc.nasa.gov/weather_prediction/GEOS-CF/).

References

Alonso, A. M., Berrendero, J. R., Hernández, A., and Justel, A.: Time Series Clustering Based on Forecast Densities, Computational Statistics & Data Analysis, 51(2), 762–776., https://doi.org/10.1016/j.csda.2006.04.035, 2006.

Banta, R. M., Senff, C. J., Nielsen-Gammon, J., Darby, L. S., Ryerson, T. B., Alvarez, R. J., Sandberg, S. P., Williams, E. J., and Trainer, M: A bad air day in Houston. Bulletin of the American Meteorological Society, 86(5), 657–670. https://doi.org/10.1175/BAMS-86-5-657, 2005.

Bernier, C., Wang, Y., Estes, M., Lei, R., Jia, B., Wang, S., and Sun, J.: Clustering Surface Ozone Diurnal Cycles to Understand the Impact of Circulation Patterns in Houston, TX, Journal of Geophysical Research: Atmospheres, 124(23), 13457–13474., https://doi.org/10.1029/2019jd031725, 2019.

Caicedo, V., Rappenglueck, B., Cuchiara, G., Flynn, J., Ferrare, R., Scarino, A. J., Berkoff, T., Senff, C., Langford, A., and Lefer, B.: Bay Breeze and Sea Breeze Circulation Impacts on the Planetary Boundary Layer and Air Quality from an Observed and Modeled Discover-AQ Texas Case Study, Journal of Geophysical Research: Atmospheres, 124(13), 7359-7378, https://doi.org/10.1029/2019jd030523, 2019.

Charrad, M., Ghazzali, N., Boiteau, V., and Niknafs, A.: NBCLUST: An R package for Determining the Relevant Number of Clusters in a Data Set, Journal of Statistical Software, 61,(6), https://doi.org/10.18637/jss.v061.i06, 2014.

Christiansen, B.: Atmospheric Circulation Regimes: Can Cluster Analysis Provide the Number?, Journal of Climate, 20(10), 2229–2250., https://doi.org/10.1175/jcli4107.1, 2007.

Coggon, M. M., Gkatzelis, G. I., McDonald, B. C., Gilman, J. B., Schwantes, R. H., Abuhassan, N., Aikin, K. C., Arend, M. F., Berkoff, T. A., and Brown, S. S.: Volatile chemical product emissions enhance ozone and modulate urban chemistry, Proceedings of the National Academy of Sciences, 118,32, National Academy of Sciences, https://doi.org/10.1073/pnas.2026653118, 2021.

Couillard, M. H., Schwab, M. J., Schwab, J. J., Lu, C. H., Joseph, E., Stutsrim, B., Shrestha, B., Zhang, J., Knepp, T. N., and Gronoff, G. P., Vertical Profiles of Ozone Concentrations in the Lower Troposphere Downwind of New York City during LISTOS 2018-2019, Journal of Geophysical Research: Atmospheres, 126(23), e2021JD035108, https://doi.org/10.1029/2021JD035108, 2021.

Darby, L. S.: Cluster Analysis of Surface Winds in Houston, Texas, and the Impact of Wind Patterns on Ozone, Journal of Applied Meteorology, 44(12), 1788–1806., https://doi.org/10.1175/jam2320.1, 2005.

Davis, R. E., Normile, C. P., Sitka, L., Hondula, D. M., Knight, D. B., Gawtry, S. P., and Stenger, P. J.: A Comparison of Trajectory and Air Mass Approaches to Examine Ozone Variability, Atmospheric Environment, 44(1), 64–74., https://doi.org/10.1016/j.atmosenv.2009.09.038, 2010.

De Young, R., Carrion, W., Ganoe, R., Pliutau, D., Gronoff, G., Berkoff, T., and Kuang, S.: Langley Mobile Ozone LIDAR: Ozone and Aerosol Atmospheric Profiling for Air Quality Research, Applied Optics, 56(3), 721, https://doi.org/10.1364/ao.56.000721, 2017.

Dreessen, J., Orozco, D., Boyle, J., Szymborski, J., Lee, P., Flores, A., and Sakai, R. K.: Observed Ozone over the Chesapeake Bay Land-Water Interface: The Hart-Miller Island Pilot Project, Journal of the Air & Waste Management Association, 69, (11), 1312–1330, https://doi.org/10.1080/10962247.2019.1668497, 2019.

EPA NEI (National Emissions Inventory v1): Air Pollutant Emission Trends Data, available at: http://www.epa.gov/ttn/chief/trends/index.html last access: 23 June 2015.

Farris, B. M., Gronoff, G. P., Carrion, W., Knepp, T., Pippin, M., and Berkoff, T. A.: Demonstration of an off-Axis Parabolic Receiver for near-Range Retrieval of Lidar Ozone Profiles, Atmospheric Measurement Techniques, 12(1), 363–370, https://doi.org/10.5194/amt-12-363-2019, 2019.

Gelaro, R., Gelaro, R., McCarty, W., Suárez, M. J., Todling, R., Molod, A., Takacs, L., Randles, C. A., Darmenov, A., Bosilovich, M. G. Reichle, R., Wargan, K., Coy, L., Cullather, R., Draper, C., Akella, S., Buchard, V., Conaty, A., da Silva, A. M., Gu, W., Kim, G-K., Koster, R., Lucchesi, R., Merkova, D., Nielsen, J. E., Partyka, G., Pawson, S., Putman, W., Rienecker, M., Schubert, S. D., Sienkiewicz, M., and Zhao, B.: The Modern-Era Retrospective Analysis for Research and Applications, Version 2 (Merra-2), Journal of Climate, 30(14), 5419–5454., https://doi.org/10.1175/jcli-d-16-0758.1, 2017.

Gronoff, G., Robinson, J., Berkoff, T., Swap, R., Farris, B., Schroeder, J., Halliday, H.S., Knepp, T., Spinei, E., Carrion, W., Adcock, E.E., Johns, Z., Allen, D., Pippin, M.: A Method for Quantifying near Range Point Source Induced O3 Titration Events Using Co-Located Lidar and Pandora Measurements, Atmospheric Environment, 204, 43–52, https://doi.org/10.1016/j.atmosenv.2019.01.052, 2019

Gronoff, G., Berkoff, T., Knowland, K.E., Lei, L., Shook, M., Fabbri, B., Carrion, W., Langford, A. O.: Case study of stratospheric Intrusion above Hampton, Virginia: lidar-observation and modeling analysis, Atmospheric Environment, 259,118498, 1352-2310, https://doi.org/10.1016/j.atmosenv.2021.118498, 2021.

Han, J. and Kamber, M.: Data mining: concepts and techniques, San Francisco: Morgan Kaufmann Publishers, 2001.

Holmes, C. D., Bertram, T. H., Confer, K. L., Graham, K. A., Ronan, A. C., Wirks, C. K., and Shah, V.: The Role of Clouds in the Tropospheric NO*x* Cycle: A New Modeling Approach for Cloud Chemistry and Its Global Implications, Geophys. Res. Lett., 46, 4980–4990, https://doi.org/10.1029/2019GL081990, 2019.

Hu, L., Keller, C. A., Long, M. S., Sherwen, T., Auer, B., Da Silva, A., Nielsen, J. E., Pawson, S., Thompson, M. A., Trayanov, A. L., Travis, K. R., Grange, S. K., Evans, M. J., and Jacob, D. J.: Global simulation of tropospheric chemistry at 12.5 km resolution: performance and evaluation of the GEOS-Chem chemical module (v10-1) within the NASA GEOS Earth system model (GEOS-5 ESM), Geosci. Model Dev., 11, 4603–4620, https://doi.org/10.5194/gmd-11-4603-2018, 2018.

Kaufman, L. and Rousseeuw, P.: Finding groups in data: An introduction to cluster analysis, New York, Wiley, 1990.

Keller, C.A., Knowland, K.E., Duncan, B.N., Liu, J., Anderson, D.C., Das, S., Lucchesi, R.A., Lundgren, E.W., Nicely, J.M., Nielsen, E., Ott, L.E., Saunders, E., Strode, S.A., Wales, P.A., Jacob, D.J., and Pawson, S.: Description of the NASA Geos Composition Forecast Modeling System GEOS-CF v1.0, Journal of Advances in Modeling Earth Systems, 13(4), https://doi.org/10.1029/2020ms002413, 2021.

Knowland, K.E., Keller, C.A., Lucchesi, R.: File specification for GEOS-CF products, GMAO office note No. 17 (version 1.0). available from: https://gmao.gsfc.nasa.gov/pubs/office_notes.php, 32, 2019.

Knowland, K. E., Keller, C. A., Wales, P. A., Wargan, K., Coy, L., Johnson, M. S., Liu, J., Lucchesi, R. A., Eastham, S. D., Fleming, E. L., Liang, Q., Leblanc, T., Livesey, N. J., Walker, K. A., Ott, L. E., and Pawson, S.: NASA GEOS Composition Forecast Modeling System GEOS-CF v1.0: Stratospheric Composition, 14(6), e2021MS002852, https://doi.org/10.1002/essoar.10508148.1, 2021.

Lawson, R. G., and Jurs, P. C.: New Index for Clustering Tendency and Its Application to Chemical Problems, Journal of Chemical Information and Computer Sciences, 30(1), 36–41., https://doi.org/10.1021/ci00065a010, 1990.

Leblanc, T., Brewer, M. A., Wang, P. S., Granados-Muñoz, M. J., Strawbridge, K. B., Travis, M., Firanski, B., Sullivan, J. T., McGee, T. J., Sumnicht, G. K., Twigg, L. W., Berkoff, T. A., Carrion, W., Gronoff, G., Aknan, A., Chen, G., Alvarez, R. J., Langford, A. O., Senff, C. J., Kirgis, G., Johnson, M. S., Kuang, S., and Newchurch, M. J.: Validation of the TOLNet lidars: the Southern California Ozone Observation Project (SCOOP), Atmos. Meas. Tech., 11, 6137–6162, https://doi.org/10.5194/amt-11-6137-2018, 2018.

Lei, L., Berkoff, T. A., Gronoff, G., Su, J., Nehrir, A. R., Wu, Y., Moshary, F., and Kuang, S.: Retrieval of UVB aerosol extinction profiles from the ground-based Langley Mobile Ozone Lidar (LMOL) system, Atmos. Meas. Tech., 15, 2465–2478, https://doi.org/10.5194/amt-15-2465-2022, 2022.

Li, W., Wang, Y., Bernier, C., and Estes, M.: Identification of Sea Breeze Recirculation and Its Effects on Ozone in Houston, TX, during Discover-Aq 2013, Journal of Geophysical Research: Atmospheres, 125(22), https://doi.org/10.1029/2020jd033165, 2020.

Little, R. J., A., and Rubin, D., B.: Statistical Analysis with Missing Data. Second ed., Wiley, 1987.

Mao, J., Zhao, T., Keller, C. A., Wang, X., McFarland, P. J., Jenkins, J. M., and Brune, W. H.: Global Impact of Lightning-Produced Oxidants, Geophys. Res. Lett., 48, https://doi.org/10.1029/2021GL095740, 2021.

McDuffie, E. E., Smith, S. J., O'Rourke, P., Tibrewal, K., Venkataraman, C., Marais, E. A., Zheng, B., Crippa, M., Brauer, M., and Martin, R. V.: A global anthropogenic emission inventory of atmospheric pollutants from sector- and fuel-specific sources (1970–2017): an application of the Community Emissions Data System (CEDS), Earth Syst. Sci. Data, 12, 3413–3442, https://doi.org/10.5194/essd-12-3413-2020, 2020.

Orbe, C., Oman, L. D., Strahan, S. E., Waugh, D. W., Pawson, S., Takacs, L. L., and Molod, A. M.: Large-scale atmospheric transport in GEOS replay simulations, J. Adv. Model. Earth Syst., 9, 2545–2560, https://doi.org/10.1002/2017MS001053, 2017.

Ring, A. M., Canty, T. P., Anderson, D. C., Vinciguerra, T. P., He, H., Goldberg, D. L., Ehrman, S. H., Dickerson, R. R., and Salawitch, R. J.: Evaluating commercial marine emissions and their role in air quality policy using observations and the CMAQ model, Atmospheric Environment, 173, 96-107, https://doi.org/10.1016/j.atmosenv.2017.10.037, 2018.

Stauffer R.M., Thompson A.M., and Witte J.C.: Characterizing Global Ozonesonde Profile Variability from Surface to the UT/LS with a Clustering Technique and MERRA-2 Reanalysis, J Geophys Res Atmos. 123(11):6213-6229. https://doi.org/10.1029/2018JD028465, 2018.

Strode, S. A., Ziemke, J.R., Oman, L. D., Lamsal, L. N., Olsen, M. A., and Liu, J.: Global changes in the diurnal cycle of surface ozone, Atmospheric Environment, 199, 323-333, https://doi.org/10.1016/j.atmosenv.2018.11.028, 2019.

Sullivan, J. T., McGee, T. J., Leblanc, T., Sumnicht, G. K., and Twigg, L. W.: Optimization of the GSFC TROPOZ DIAL retrieval using synthetic lidar returns and ozonesondes – Part 1: Algorithm validation, Atmos. Meas. Tech., 8, 4133–4143, https://doi.org/10.5194/amt-8-4133-2015, 2015.

Sullivan, J.T., McGee, T.J., DeYoung, R., Twigg, L.W., Sumnicht, G.K., Pliutau, D., Knepp, T., and Carrion, W.: Results from the NASA GSFC and LaRC Ozone Lidar intercomparison: new mobile tools for atmospheric research, J. Atmos. Ocean. Technol., 32 (10), 1779-1795, https://doi.org/10.1175/JTECH-D-14-00193.1, 2015.

Thompson, A. M., Stauffer, R. M., Miller, S. K., Martins, D. K., Joseph, E., Weinheimer, A. J., and Diskin, G. S.: Ozone profiles in the Baltimore-Washington region (2006-2011): satellite comparisons and DISCOVER-AQ observations, J Atmos Chem., 72(3-4), 393-422. https://doi.org/10.1007/s10874-014-9283-z, 2015.

Torgo, L.: Data Mining with R, Chapman & Hall/CRC Data Mining and Knowledge Discovery Series, https://doi.org/10.1201/b10328, 2010.

Wang, L., Newchurch, M. J., Alvarez, R. J., Berkoff, T. A., Brown, S. S., Carrion, W., De Young, R. J., Johnson, B. J., Ganoe, R., Gronoff, G., Kirgis, G., Kuang, S., Langford, A. O., Leblanc, T., McDuffie, E. E., McGee, T. J., Pliutau, D., Senff,

C. J., Sullivan, J. T., Sumnicht, G., Twigg, L. W., and Weinheimer, A. J.: Quantifying TOLNet Ozone Lidar Accuracy during the 2014 DISCOVER-AQ and FRAPPÉ Campaigns. Atmos Meas Tech, 10(10), 3865-3876, http://doi.org/10.5194/amt-10-3865-2017. 2017.

Wang, X., Jacob, D. J., Downs, W., Zhai, S., Zhu, L., Shah, V., Holmes, C. D., Sherwen, T., Alexander, B., Evans, M. J., Eastham, S. D., Neuman, J. A., Veres, P. R., Koenig, T. K., Volkamer, R., Huey, L. G., Bannan, T. J., Percival, C. J., Lee, B. H., and Thornton, J. A.: Global tropospheric halogen (Cl, Br, I) chemistry and its impact on oxidants, Atmospheric Chem. Phys., 21, 13973–13996, https://doi.org/10.5194/acp-21-13973-2021, 2021.

Wu, Y., Nehrir, A. R., Ren, X., Dickerson, R. R., Huang, J., Stratton, P. R., Gronoff, G., Kooi, S. A., Collins, J. E., and Berkoff, T. A.: Synergistic aircraft and ground observations of transported wildfire smoke and its impact on air quality in New York City during the summer 2018 LISTOS campaign, Science of The Total Environment, 773,145030, https://doi.org/10.1016/j.scitotenv.2021.145030, 2021.